# Poroelastic modeling of fracture-seismic wave interaction

Seiji NAKAGAWA

Lawrence Berkeley National Laboratory

**ABSTRACT**

Rock containing a compliant, fluid-filled fracture can be viewed as one case of heterogeneous poroelastic media. When this fracture is subjected to seismic waves, a strong contrast in the elastic stiffness between the fracture itself and the background can result in enhanced grain-scale local fluid flow. Because this flow—relaxing the pressure building up within the fracture—can increase the dynamic compliance of the fracture and change energy dissipation (attenuation), the scattering of seismic waves can be enhanced. Previously, for a flat, infinite fracture, we derived poroelastic seismic boundary conditions that describe the relationship between a finite jump in the stress and displacement across a fracture, expressed as a function of the stress and displacement at the boundaries. In this paper, we use these boundary conditions to determine frequency-dependent seismic wave transmission and reflection coefficients. Fluid-filled fractures with a range of mechanical and hydraulic properties are examined. From parametric studies, we found that the hydraulic permeability of a fracture fully saturated with water has little impact on seismic wave scattering. In contrast, the seismic response of a partially water-saturated fracture and a heterogeneous fracture filled with compliant liquid (e.g., supercritical $CO_2$) depended on the fracture permeability.

*Keywords: Fracture, Seismic wave, Poroelasticity, Permeability, boundary condition*

## 1. INTRODUCTION

A fracture serves as an efficient conduit for fluid transport in low-permeability rock. This makes characterizing the hydraulic properties of fractures essential for predicting subsurface fluid transport. It is often desirable to estimate the permeability of fractures at depth from geophysical measurements (seismic methods, in particular), although currently, no well-established effective and practical techniques exist. Because seismic properties of fluid-bearing, poroelastic materials are generally affected by their permeability (e.g., Biot, 1956ab; Johnson et al., 1978), in principle, the permeability of a fracture should also be reflected in its interaction with seismic waves.

Previously, Nakagawa and Schoenberg (2007) derived a simple model (in the form of boundary conditions) for predicting how a fracture with a range of mechanical and hydraulic properties affects scattering of seismic waves. This model assumed a fracture to be a thin layer of homogeneous poroelastic material embedded within a homogeneous background. Surprisingly, the model predicted that the permeability of a fracture (along the fracture plane) did not affect the scattering of seismic waves. This is a somewhat disappointing result, if we want to use seismic waves to determine the permeability of a fracture.

Note, however, that the simplified conceptual model for a fracture used in the Nakagawa and Schoenberg (2007)'s model—a fracture envisioned as a flat, homogeneous, poroelastic layer embedded within a background poroelastic medium—may not be adequate for predicting the behavior of a real fracture. For fracture-parallel fluid flow to occur between high and low-pressure regions within a fracture, the length scale of wave-induced pressure variation (pressure diffusion length, or Biot's slow-wave wavelength within the fracture) has to be comparable to or longer than the distance between neighboring peaks and troughs of pressure, along the fracture plane. This is usually not the case for a thin, homogeneous fracture in which the speed of the wave-induced pressure propagation is significantly slower than the incident waves: the fluid is practically "frozen" in the fracture-parallel direction.

In contrast, if the mechanical and hydraulic properties of a fracture are heterogeneously distributed along the fracture plane, the intrinsic pressure diffusion length within the fracture may become comparable to or surpass the length scale of the heterogeneity, resulting in relaxation of wave-induced pressure (Figure 1). In recent years, the effects of "mesoscale" (larger than grain/pore size but smaller than the wavelength of propagating waves) heterogeneity in rock on enhanced seismic velocity dispersion and attenuation have been widely recognized (e.g., Dutta and Odé, 1979ab; Norris, 1993; Johnson, 2001; Pride and Berryman, 2003ab). Therefore, we should be able to expect the same heterogeneity-induced poroelastic behavior for a fluid-filled, heterogeneous fracture.

In this paper, we will examine how the heterogeneity within a single fracture can affect the scattering of seismic waves, particularly as a function of fracture permeability. We will first briefly review the poroelastic seismic boundary conditions derived by Nakagawa and Schoenberg (2007). Subsequently, these conditions will be extended to include the effect of fracture-parallel fluid flow. Further, an analytical framework will be built to compute plane wave scattering by a fracture with heterogeneously distributed mechanical and hydraulic properties, applying the method used by Nakagawa et al. (2004). Finally, the derived equation will be solved numerically for particular fracture models to demonstrate how different types of heterogeneity affect the fractures' seismic responses.

The results of the numerical study indicate that when a fracture is saturated with a stiff fluid (e.g., water), the seismic wave scattering is hardly affected by the fracture permeability, even when the distribution of the fracture compliance is strongly heterogeneous. However, if the compliance of the fluid is very high (e.g., supercritical $CO_2$) or the stiff fluid locally contains gas bubbles, seismic wave scattering can be affected by the (fracture-parallel) permeability.

## 2. POROELASTIC SEISMIC BOUNDARY CONDITIONS FOR A FRACTURE

In this section, we will first review the poroelastic seismic boundary conditions for a homogeneous fracture (fracture and fluid properties do not change along the fracture). Subsequently, these boundary conditions will be extended to heterogeneous fractures. In both cases, we will limit our discussions to fractures without in-filling gouge materials, or fractures with highly permeable gouge materials. This restriction allows us to assume the continuity of fluid pressure across a fracture, which greatly simplifies of the mathematical treatment.

### *2.1 Boundary conditions for a homogeneous fracture*

Nakagawa and Schoenberg's seismic boundary conditions (2007) for a fracture filled with a highly permeable material (or without such materials) are given by:

$$
\begin{aligned}
[\tau_{13}] &= 0 \\
[\tau_{23}] &= 0 \\
[\tau_{33}] &= 0 \\
[-p_f] &= 0 \\
[u_1] &= \eta_T \tau_{13} \\
[u_2] &= \eta_T \tau_{23} \\
[u_3] &= \eta_{Nd} \left\{ \tau_{33} - \alpha(-p_f) \right\} \\
[w_3] &= \eta_{Nd} \alpha \left\{ -\tau_{33} + (1/\tilde{B})(-p_f) \right\} \\
&\left( = -\alpha [u_3] + \eta_M (-p_f) \right)
\end{aligned}
\qquad , \quad (1)
$$

where the square brackets [*] indicate the difference (or jump) in the related quantity across the fracture. (A similar model was proposed by Bakulin and Molotkov [1997].) The equations assume a Cartesian coordinate system with the 1, 2-directions aligned with the fracture plane (i.e., the 3 direction is the fracture-normal direction) (Figure 2). The symbols used in these equations are summarized in Table 1.

Equation (1) was derived originally by modeling a fracture as a thin, homogeneous poroelastic layer with a well-defined thickness *h*. However, by considering the equations' physical implications and by slightly changing the interpretation of the "fracture thickness," these boundary conditions can also be applied to a fracture consisting of partial contacts between two solid halfspaces.

The physical meaning of the expressions of Equation (1) (defined for a "homogeneous fracture" with uniform distributions of the characteristic parameters) is as follows: the first four boundary conditions state continuity of total stress and fluid pressure across a fracture. The fifth and sixth conditions state proportionality between seismically induced small perturbation of shear stress and displacement jump across a fracture. The remaining expressions show the poroelastic constitutive relationships. The seventh expression represents the effective stress law (thus including the Biot-Willis effective stress coefficient $\alpha$), and the eighth and last expression states the conservation of mass by equating the volume of fluid expelled by a fracture (left-hand side of the equation) to the fluid displaced by a closing fracture (the first term in the right-hand side, including $\alpha$) and the volume changes of fluid and solid within the fracture through $\eta_M$. For a fracture modeled by a poroelastic layer, this last coefficient $\eta_M$ is defined by:

$$
\eta_M \equiv \frac{h}{M} = h\left( \frac{\alpha - \phi}{K_s} + \frac{\phi}{K_f} \right), \qquad (2)
$$

where $M$ is the Biot's storage coefficient, and $K_s$ and $K_f$ are the bulk moduli for solid and fluid within the fracture, respectively (e.g., Pride, 2003). From this definition, $\eta_M$ can be used to measure the fluid effect on the compressibility of a fracture. Note that, instead of $\eta_M$, the fracture Skempton coefficient $\tilde{B}$ (Nakagawa and Schoenberg, 2007—also see Table 1 footnote) can also be used, which quantifies how much of the total stress "uniaxially" (normally to the fracture) applied to a fracture is counteracted by fluid pressure, under undrained conditions.

For a fracture consisting of partial contacts between two solid halfspaces, we need to define two concepts related to "fracture thickness"—"mechanical thickness" $h_M$ and "hydraulic thickness" $h_H$. The $h_M$ concept is defined for the zone including the fracture asperities and a part of the background medium—the part experiencing the local perturbation of stress and deformation caused by surface heterogeneities (e.g., Myer, 2000). Therefore, defining the mechanical fracture thickness is somewhat arbitrary. The static parameters appearing within the boundary conditions ($\eta_T$, $\eta_{Nd}$, $\eta_M$, $\alpha$, and $\tilde{B}$) are defined as effective medium parameters for the materials within this thickness. This representation of fracture properties has been shown to be sufficient for describing the scattering behavior of seismic waves, as long as the thickness of the zone is much smaller than the seismic wavelengths (Schoenberg, 1980; Pyrak-Nolte et al., 1990; Rockhlin et al., 1991). In contrast, a separate fracture thickness $h_H$—which is closely related to the hydraulic permeability of the fracture—needs to be defined for studying the dynamic, flow properties. (The thickness $h_H$ is usually smaller than $h_M$.)

However, note that because the above boundary conditions expressed in Equation (1) do not depend on the permeability of a fracture, the scattering of seismic waves computed using the above equations is not affected by the fracture permeability.

*2.2 Boundary conditions for a heterogeneous fracture*

One major difference between a homogeneous fracture (represented by a poroelastic layer) and a more realistic, heterogeneous fracture is that there should be an enhanced fluid motion within a heterogeneous fracture, induced by a local fluid-pressure gradient. This is analogous to the locally induced fluid flow within a heterogeneous porous medium, which can result in a much larger seismic-wave-velocity dispersion and attenuation compared to a classical, homogeneous porous medium studied by Biot (Biot, 1956ab).

The locally induced flow can have an impact on the seismic boundary conditions in two ways, if the fluid-inertia-related effects can be neglected for the small thickness of the fracture. These are (1) the effect of viscous shear stress resulting from fluid motion within the fracture (which disrupts the continuity of shear stresses in the first and second expressions in Equation [1]), and (2) changes in the fracture-normal fluid flux caused by the flow parallel to the fracture (which modifies the fluid-flux discontinuity condition in the last expression of Equation [1]).

The first effect, however, can be ignored for fracture thicknesses that are much smaller than the length scale of local fluid-pressure variation and heterogeneity along the fracture surface. For simplicity, we assume a one-dimensional fracture with a hydraulic fracture thickness $h_H$. Also, the background is assumed to be impermeable. If the local variation of fluid pressure $\Delta(-p_f)$ occurs over a small distance $\Delta L(>>h_H)$, the average shear stress $\tau$ in this section is given (see Figure 3) by

$$|\tau| = \left|\Delta(-p_f)\right| \frac{h_H}{2\Delta L} << \left|-p_f\right|. \qquad (3)$$

Note that the effect of the fluid inertia is ignored because we are already assuming a long wavelength. Although a constant fracture thickness is assumed here, the inequality also holds for spatially varying fracture thickness. This result indicates that the fluid flow-induced shear stress can be ignored compared to the effect of induced fluid pressure within a fracture.

The second effect can be included in the last expression in Equation (1) as follows:

$$\begin{aligned}[w_3] &= -\alpha[u_3] + \eta_M(-p_f) - \partial_1\left(\overline{w}_1 h_H\right) - \partial_2\left(\overline{w}_2 h_H\right) \\ &\left(= -\alpha[u_3] + \eta_M(-p_f) - \nabla^{(2)}\cdot\left(\overline{\mathbf{w}}^{(2)} h_H\right)\right)\end{aligned} . \qquad (4)$$

The newly added third and fourth terms account for the influx of fluid at the point of consideration, from the surrounding locations within the fracture plane. The superscript (2) indicates that the related quantities are two dimensional, expanding in the 1, 2 directions. Also, the bars ("-") above the relative flow displacement $w_1$ and $w_2$ indicate averaging across the fracture thickness. The fluid flux in the fracture-parallel direction can be evaluated via Biot's solution for oscillatory flow between flat parallel walls (Biot, 1956b):

$$\dot{\overline{w}}_i = (-i\omega)\overline{w}_i = \frac{k_T(\omega)}{\eta_f}\left\{\frac{\partial(-p_f)}{\partial x_i} - \rho_f \overline{\ddot{u}}\right\} \ (i=1,2) \qquad (5)$$

where

$$k_T(\omega) = \frac{h_H^2}{4}\frac{1}{W^2}\left(1 - \frac{\tanh W}{W}\right),\ W \equiv \frac{h_H}{2}\sqrt{\frac{\omega\rho_f}{i\eta_f}} . \qquad (6)$$

Note that the first term on the right hand side of the Equation (5) represents the flow induced by a pressure gradient, and the second term represents the apparent flow caused by the moving frame of reference (background rock or fracture surfaces). For simplicity, we assume an isotropic second-rank diagonal permeability tensor for the flow parallel to the fracture:

$$\mathbf{k}^{(2)}(\omega) = \begin{bmatrix} k_T & \\ & k_T \end{bmatrix}. \qquad (7)$$

For the flow within a fracture, the components of the above matrix are defined for flow spatially averaged across the fracture thickness. Therefore, 1, 2-direction components of relative fluid flux $\dot{\overline{\mathbf{w}}}$ and acceleration $\overline{\ddot{\mathbf{u}}}$ are also averaged quantities across the fracture thickness. By introducing Equation (5) into Equation (4),

$$\begin{aligned}[w_3] &= -\alpha[u_3] + \eta_M(-p_f) \\ &\quad -\nabla^{(2)}\cdot\left(\frac{k_T(\omega)}{-i\omega\eta_f} h_H\left\{\nabla^{(2)}(-p_f) - \omega^2\rho_f\overline{\mathbf{u}}^{(2)}\right\}\right) \\ &= -\alpha\eta_{N_a}\tau_{33} \\ &+\left\{\alpha\eta_{N_a} + \eta_M + \frac{1}{i\omega}\nabla^{(2)}\cdot\left(\varsigma(\omega)\nabla^{(2)}\right)\right\}(-p_f), \\ &+i\omega\rho_f\nabla^{(2)}\cdot\left(\varsigma(\omega)\overline{\mathbf{u}}^{(2)}\right)\end{aligned} \qquad (8)$$

where we defined a new, spatially varying characteristic parameter (fracture permissivity)

$$\varsigma(\omega) \equiv \frac{k_T(\omega)h_H}{\eta_f} . \qquad (9)$$

Note that this parameter can become a second-rank tensor through a related permeability tensor, $\mathbf{k}^{(2)}(\omega)$, if necessary.

Summarizing the results, the boundary conditions for a heterogeneous, fluid-filled fracture are

$$\boldsymbol{\tau}^{+}(x_1,x_2)=\boldsymbol{\tau}^{-}(x_1,x_2)\,, \tag{10}$$

$$\begin{aligned}&\mathbf{u}^{+}(x_1,x_2)-\mathbf{u}^{-}(x_1,x_2)\\&=\left\{\boldsymbol{\eta}(x_1,x_2)-\frac{1}{i\omega}\boldsymbol{\eta}'(x_1,x_2)\right\}\boldsymbol{\tau}^{+}(x_1,x_2)\\&+i\omega\boldsymbol{\eta}''(x_1,x_2)\left\{\mathbf{u}^{+}(x_1,x_2)+\mathbf{u}^{-}(x_1,x_2)\right\}\\&(x_3\to\pm h_M/2,\ \pm h_H/2)\end{aligned}\,, \tag{11}$$

where

$$\boldsymbol{\tau}^{\pm}\equiv\begin{bmatrix}\tau_{31} & \tau_{32} & \tau_{33} & -p_f\end{bmatrix}^T, \tag{12}$$

$$\mathbf{u}^{\pm}\equiv\begin{bmatrix}u_1 & u_2 & u_3 & w_3\end{bmatrix}^T, \tag{13}$$

$$\boldsymbol{\eta}(x_1,x_2)\equiv\begin{bmatrix}\eta_T & & & \\ & \eta_T & & \\ & & \eta_{Nd} & -\alpha\eta_{Nd}\\ & & -\alpha\eta_{Nd} & \alpha\eta_{Nd}+\eta_M\end{bmatrix}, \tag{14}$$

$$\boldsymbol{\eta}'(x_1,x_2)\equiv\begin{bmatrix}0 & & & \\ & 0 & & \\ & & 0 & \\ & & & \nabla^{(2)}\cdot\left(\varsigma(\omega)\nabla^{(2)}\right)\end{bmatrix}, \tag{15}$$

$$\boldsymbol{\eta}''(x_1,x_2)\equiv\frac{\rho_f}{2}\begin{bmatrix}\partial_1\varsigma(\omega)\cdot & & & \\ & \partial_2\varsigma(\omega)\cdot & & \\ & & 0 & \\ & & & 0\end{bmatrix}. \tag{16}$$

The superscripts "+" and "-" indicate the individual sides of the fracture. (Note that the precise location where the boundaries are defined is somewhat ambiguous, because the fracture thickness $h_M$ and $h_H$ should be defined through mechanical and hydrological properties of a fracture, rather than its actual geometry.) Also, in Equation (11), the solid frame displacement (or acceleration) along the fracture is approximated as an average of the displacements across the fracture as $\overline{\mathbf{u}}=\left(\mathbf{u}^{+}+\mathbf{u}^{-}\right)/2$.

## 3. COMPUTATION OF WAVE SCATTERING BY A HETEROGENEOUS FRACTURE

To examine the scattering of plane waves by a heterogeneous fracture, the above seismic boundary conditions are assumed to be valid at each location on the fracture. In this model, the heterogeneity is represented by spatially varying characteristic fracture parameters such as fracture compliances $\eta_{Nd}$, $\eta_T$, $\eta_M$, Biot-Willis coefficient $\alpha$, fracture Skempton coefficient $\tilde{B}$, and fracture-parallel hydraulic permissivity $\varsigma(\omega)$. When spatial Fourier transforms are applied to Equations (10) and (11), the multiplications between the variables and the characteristic fracture parameters become convolutions in the wavenumber domain, which represent multiple scattering of waves involving both specular and nonspecular scattering (resulting in conversions in wavenumber)

(Nakagawa et al., 2004). Representing the transformed variables by a tilde ("~"), the transformed equations are

$$\tilde{\boldsymbol{\tau}}^{+} = \tilde{\boldsymbol{\tau}}^{-} + \tilde{\boldsymbol{\tau}}^{I}, \tag{17}$$

$$\begin{aligned}&\tilde{\mathbf{u}}^{+} - \left(\tilde{\mathbf{u}}^{-} + \tilde{\mathbf{u}}^{I}\right)\\ &= \left[\tilde{\boldsymbol{\eta}}(k_1,k_2) - \frac{1}{i\omega}\tilde{\boldsymbol{\eta}}'(k_1,k_2)\right] * \tilde{\boldsymbol{\tau}}^{+}\\ &+ i\omega\tilde{\boldsymbol{\eta}}''(k_1,k_2) * \left[\tilde{\mathbf{u}}^{+} + \left(\tilde{\mathbf{u}}^{-} + \tilde{\mathbf{u}}^{I}\right)\right]\end{aligned}. \tag{18}$$

Note that, in the above equations, the superscripts + and – indicate the direction of wave propagation ("+"="down-going", "–"="up-going"), rather than the sides of a fracture. The superscript "*I*" indicates a plane wave propagating in the positive $x_3$ direction. The transformed stress and displacement vectors are a function of wavenumbers $(k_1,k_2)$. Also, the transformed matrices $\tilde{\boldsymbol{\eta}}'$ and $\tilde{\boldsymbol{\eta}}''$ in Equation (18) can involve spatial derivative operators that must be treated carefully when convolved with stress and displacement vectors.

In matrix form, the displacement and stress (pressure) components of plane waves can be given by

$$\tilde{\mathbf{u}} \equiv \begin{bmatrix}\tilde{u}_1\\ \tilde{u}_2\\ \tilde{u}_3\\ \tilde{w}_3\end{bmatrix} = \mathbf{U}^{\pm}\mathbf{E}^{\pm}(x_3)\mathbf{a}^{\pm}\exp i(k_1x_1 + k_2x_2 - \omega t), \tag{19}$$

$$\tilde{\boldsymbol{\tau}} \equiv \begin{bmatrix}\tilde{\tau}_{13}\\ \tilde{\tau}_{23}\\ \tilde{\tau}_{33}\\ -\tilde{p}_f\end{bmatrix} = i\omega\mathbf{S}^{\pm}\mathbf{E}^{\pm}(x_3)\mathbf{a}^{\pm}\exp i(k_1x_1 + k_2x_2 - \omega t). \tag{20}$$

$\mathbf{U}^{\pm}$ and $\mathbf{S}^{\pm}$ are the displacement and stress coefficient matrices, respectively, which relate the amplitudes of two shear waves and fast and slow compressional waves, given by the coefficient vector $\mathbf{a}^{\pm}$, to the displacement and stress (and pressure) on the fracture surfaces. $\mathbf{E}^{\pm}$ are the diagonal phase-advance matrices. [Explicit forms of these matrices can be found in Nakagawa and Schoenberg (2007).] In the following derivations, I will take advantage of the fact that if the stress vectors were used as primary variables, the continuity of total stress vector across a fracture [Equations (10) and (17)] results in simpler equations. On the fracture, $\mathbf{E}^{\pm}$=**I**(identity matrix). Therefore, from Equations (19) and (20),

$$\mathbf{a}^{\pm} = \frac{1}{i\omega}\left(\mathbf{S}^{\pm}\right)^{-1}\tilde{\boldsymbol{\tau}}^{\pm}, \tag{21}$$

$$\therefore \tilde{\mathbf{u}}^{\pm} = \frac{1}{i\omega}\mathbf{U}^{\pm}\left(\mathbf{S}^{\pm}\right)^{-1}\tilde{\boldsymbol{\tau}}^{\pm}. \tag{22}$$

Introducing Equation (22) into the matrix Equation (18),

$$\begin{aligned}&\mathbf{U}^{+}\left(\mathbf{S}^{+}\right)^{-1}\tilde{\boldsymbol{\tau}}^{+} - \left\{\mathbf{U}^{-}\left(\mathbf{S}^{-}\right)^{-1}\tilde{\boldsymbol{\tau}}^{-} + \mathbf{U}^{+}\left(\mathbf{S}^{+}\right)^{-1}\tilde{\boldsymbol{\tau}}^{I}\right\}\\ &= i\omega\tilde{\boldsymbol{\eta}}(k_1,k_2) * \tilde{\boldsymbol{\tau}}^{+} - \tilde{\boldsymbol{\eta}}'(k_1,k_2) * \tilde{\boldsymbol{\tau}}^{+}\\ &+ i\omega\tilde{\boldsymbol{\eta}}''(k_1,k_2) * \left\{\mathbf{U}^{+}(\mathbf{S}^{+})^{-1}\tilde{\boldsymbol{\tau}}^{+} + \mathbf{U}^{-}(\mathbf{S}^{-})^{-1}\tilde{\boldsymbol{\tau}}^{-} + \mathbf{U}^{+}(\mathbf{S}^{+})^{-1}\tilde{\boldsymbol{\tau}}^{I}\right\}\end{aligned}. \tag{23}$$

Combining Equations (23) and (17),

$$\left\{\mathbf{H} - i\omega\left(\tilde{\boldsymbol{\eta}}^{*} + \tilde{\boldsymbol{\eta}}''^{*}\mathbf{G}\right) + \tilde{\boldsymbol{\eta}}'^{*}\right\}\tilde{\boldsymbol{\tau}}^{+} = \left(\mathbf{I} + i\omega\tilde{\boldsymbol{\eta}}''^{*}\right)\mathbf{H}\tilde{\boldsymbol{\tau}}^{I} \quad , \quad (24)$$

where

$$\mathbf{H} \equiv \mathbf{U}^{+}(\mathbf{S}^{+})^{-1} - \mathbf{U}^{-}(\mathbf{S}^{-})^{-1} , \quad (25)$$

$$\mathbf{G} \equiv \mathbf{U}^{+}(\mathbf{S}^{+})^{-1} + \mathbf{U}^{-}(\mathbf{S}^{-})^{-1} . \quad (26)$$

The matrix-vector multiplications $\mathbf{G}\tilde{\boldsymbol{\tau}}^{+}$ and $\mathbf{H}\tilde{\boldsymbol{\tau}}^{I}$ in Equation (24) must be performed before the wavenumber convolutions indicated by "*." For a spatially periodic fracture, the above equation can be expressed in a discrete form. In this case, the convolution operators are replaced by matrices as $\tilde{\boldsymbol{\eta}}^{*} \to \hat{\tilde{\boldsymbol{\eta}}}$, $\tilde{\boldsymbol{\eta}}'^{*} \to \hat{\tilde{\boldsymbol{\eta}}}'$, and $\tilde{\boldsymbol{\eta}}''^{*} \to \hat{\tilde{\boldsymbol{\eta}}}''$. Therefore, Equation (24) becomes

$$\left\{\hat{\mathbf{H}} - i\omega\left(\hat{\tilde{\boldsymbol{\eta}}} + \hat{\tilde{\boldsymbol{\eta}}}''\hat{\mathbf{G}}\right) + \hat{\tilde{\boldsymbol{\eta}}}'\right\}\hat{\tilde{\boldsymbol{\tau}}}^{+} = \left(\hat{\mathbf{I}} + i\omega\hat{\tilde{\boldsymbol{\eta}}}''\right)\hat{\mathbf{H}}\hat{\tilde{\boldsymbol{\tau}}}^{I} . \quad (27)$$

The solution of the scattering problem can be obtained numerically by solving this matrix equation for a given spatial distribution of fracture properties and an incident wave.

## 4. EXAMPLES

The solution of the scattering problem formulated in the previous section can be obtained for a flat, two-dimensional fracture within a homogeneous background. However, for computational reasons, we will examine only one-dimensional fractures in the following examples. Also, these examples are computed only for an incident (Biot's) fast P wave, and only the amplitude of reflected fast P wave is examined (Note: This amplitude is obtained for the coherent component [specular component] of the reflected waves).

### *4.1 Model fracture*

In the following examples, we assume a simple, one-dimensional fracture with smoothly varying local fracture properties. The material properties of the background poroelastic medium are summarized in Table 2. The examples in the following sections were computed for an underground reservoir used for geological $CO_2$ sequestration, and the material properties are given for elevated temperature and pressure ($T$=55$^{o}$C, $P$=15 MPa).

To specify the fracture model, we first assume a "hydraulic fracture width $h_H$" profile given by

$$h_H(x_1) = 10^{-4+\cos\left(2\pi\frac{x_1}{L}\right)} \text{ (m)} \quad (28)$$

where $L$ is the one periodic length of the fracture. At each point along the fracture, this width is used to calculate the local fracture permeability $k_T$ (and permissivity $\varsigma$) via Equation (6) and the storage compliance $\eta_M$ via Equation (2), for different types of fluids and local fluid saturation. To obtain a fracture compliance distribution correlated to $h_H$, we simply assume that both dry-normal and shear compliances are given by $\eta_T$, $\eta_{Nd}$ [m/Pa]=$10^{-6}\times h_H$ [m]. Although this model is admittedly arbitrary, it should suffice for examining the salient nature of seismic wave scattering by a fluid-filled fracture.

In each example, we will use background materials with two different permeability values (as shown in Table 2) and a range of fracture permeability. The permeability of the fracture is specified by multiplying a reduction factor $F$ (=0.001, 0.01, 0.1, and 1.0) to the reference fracture

permissivity $\varsigma_{ref}$ (obtained using Equation [9]). Physically, this can be viewed as the permeability-reducing effect of rough fracture surfaces and/or gouge material. The Biot-Willis coefficient for the fracture $\alpha$ is assumed to be 1.

*4.2 Homogeneous fracture:Saturated by water*

In the first example, we examine a homogeneous, water-saturated fracture. For this fracture, the hydraulic width is assumed to be 1 mm.

Reflection coefficients of fast P waves for a normally incident wave are shown in Figure 4a, as a function of wave frequency. Each curve corresponds to different background permeability (high=10 μD or low=10 D). From the plot, the amplitude of the waves is higher for the high-permeability background. This is because the wave-induced fluid pressure within a fracture is dissipated into the background medium, which effectively increases the (normal) compliance of the fracture. In contrast, the permeability of the fracture itself has little impact on the amplitudes of reflected waves, because the fluid cannot move along the fracture for the normally incident P wave.

When a P wave is obliquely incident upon a fluid-filled fracture, the pressure gradient induced along the fracture should result in fluid flow, which changes the P-wave reflection depending on the fracture permeability. Figure 4b shows the reflection coefficients for obliquely ($45^o$) incident fast P-waves. Although a range of fracture permissivity values are used, the results are all indistinguishable from one another, for the both high and low background permeability cases. This result indicates that in contrast to the large differences caused by the background permeability, the fracture permeability (permissivity) still has little impact on the reflection amplitude for obliquely incident P waves.

*4.2 Homogeneous fracture:Saturated by water*

As discussed in the Introduction, the lack of sensitivity to the (fracture parallel) fracture permeability can be attributed to the inability of fluid to move between a peak and a trough of pressure within a homogeneous fracture. Therefore, if a heterogeneous distribution of fracture compliance and fracture width result in a fluid pressure distribution with a much shorter length scale, the fluid may be able to move within a fracture, making scattering of the wave fracture-permeability dependent.

To examine this possibility, reflections of normally incident, fast P waves were computed for a water-saturated, heterogeneous fracture, using the model derived via Equation (28). Figure 5 shows a schematic view of the periodic, one-dimensional, heterogeneous fracture. The dry normal fracture compliance and fracture storage compliance distributions are shown for one period ($L$=0.1 m) along the fracture (Figure 6). Note that we assume that the shear fracture compliance is identical to the dry normal compliance at each point.

Contrary to our expectations, the amplitudes of reflected waves were not significantly affected by fracture permeability. Figure 7 shows qualitatively the same results as the homogeneous fracture case, showing large increases in P-wave reflection for larger background permeability, but little change for a range of fracture permeability.

*4.2 Heterogeneous fracture:Partially saturated by water*

In this example, using the same fracture model, the fluid saturation of the fracture was locally reduced down to 50% over a small range within the fracture (Figure 8). This resulted in locally increased fracture storage compliance via Equation (2) ($K_f$ was reduced by volume averaging between fluid and gas—Figure 9).

For the low-permeability background case, an introduction of a small amount of compliant gas (air under T=55 $^{o}$C and P=15 MPa) dramatically increased the compliance of the fracture, resulting in a higher reflection amplitude than the fully saturated fracture (Figure 10). Particularly, for the low-permeability background, the reflection amplitude shows a transition between high-reflection to low reflection regimes. Interestingly, the transition frequency is dependent on the fracture permeability (permissivity), which indicates that the flow within a fracture plays a role in altering the reflection amplitude.

*4.3 Heterogeneous fracture:Saturated by supercritical $CO_2$*

The overall compliance of a fracture can also be reduced by replacing the water within the fracture by a more compliant fluid. At the given T, P state, $CO_2$ is supercritical, with much higher compliance and lower viscosity than water (bulk modulus=0.0726 GPa, viscosity=$5.12\times10^{-5}$ Pa·s). The compliance distributions are shown in Figure 11.

Figure 12 shows the resulting reflection amplitudes. Although the effect of fracture-permeability difference for the low-permeability background case is not as dramatic as the partially saturated water, the overall reflection amplitudes are much larger than the water-saturated fracture.

## 4. DISCUSSIONS AND CONCLUSIONS

This paper presents a set of displacement-stress boundary conditions for computing the scattering of seismic waves by a fluid-filled, heterogeneous fracture. The heterogeneity of the fracture is represented by a distribution of characteristic fracture parameters (fracture compliances, storage compliance, hydraulic width, [along-fracture] permissivity, Biot-Willis coefficient).

The examples for seismic wave scattering (fast P-wave reflections) computed using this model showed some interesting characteristics of interaction between seismic waves and a fluid-filled fracture.

When a fracture is embedded in a high-permeability background, the reflection of the wave can be significantly large compared to a fracture within a low-permeability (or impermeable) background. This is because the fluid pressure within a fracture can dissipate into the background, increasing the overall normal compliance of the fracture.

For a low-permeability background, the permeability of the fracture itself can play a significant role, because the degree of pressure dissipation within a fracture determines the overall compliance of the fracture. In Figure 13, normalized amplitude and pressure distributions (to the maximum value in each profile) at 316 Hz are shown for the background and fracture permeabilities (permissivity) used in the previous section. For the normal-incidence cases, increasing the fracture permeability generally makes the amplitude profile flatter and the phase profile more even.

This demonstrates that the fracture permeability is indeed controlling the pressure dissipation in the fracture. For the case of a homogeneous, water-saturated fracture with an obliquely incident wave (Figure 13a), the changes in the profiles are minimal. This seems to indicate that the fluid does not flow within the fracture. The heterogeneous, water-filled fracture does show some changes, although the relative magnitude of the changes is small, possibly because the low compliance of the fluid does not allow a large displacement.

In contrast, the fractures partially saturated with water and with supercritical $CO_2$ exhibit very large changes in the pressure amplitude and phase profile (Figure 13c and d). In both cases, large pressures are found around the low $\eta_{Nd}$ and small $h_H$ area (or fracture “asperities”) for low-permeability fractures. These high pressures are dissipated into low-pressure areas between the asperities. Essentially, this is the “squirt flow” effect (e.g., Dvorkin et al., 1994) for a fracture.

In summary, the amplitude behavior of a fast P-wave reflected by a fluid-filled fracture can be understood as follows (Figure 14): In a low-permeability background, the frequency and

permeability of a fracture determine whether the fracture is in a “relaxed” or “unrelaxed” regime. Larger reflection amplitudes result from the “relaxed” regime, since the overall fracture compliance is larger. If the background permeability is large, the reflection amplitude can be even larger (owing to the pressure dissipation into the background), and the fracture permeability can lose its effect on the wave reflection.

Finally, for the case when a compliant liquid (supercritical $CO_2$) is saturating a fracture, the enhanced compliance of a fracture allows more fluid flow, which increases the compliance of the fracture—and hence the reflection of seismic waves and permeability sensitivity. This last result is particularly important for discriminating the infiltration of the $CO_2$ phase within fractures during geological sequestration of $CO_2$.

## ACKNOWLEDGMENTS

This research has been supported by the Office of Science, Office of Basic Energy Sciences, Division of Chemical Sciences of the U.S. Department of Energy under Contract No. DE-AC02-05CH11231. The author thanks Dr. Jonathan Ajo-Franklin (Lawrence Berkeley National Laboratory) for computing the properties of supercritical $CO_2$.

**REFERENCES**


Bakulin, A., and L. Molotkov, 1997, Poroelastic medium with fractures as limiting case of stratified poroelastic medium with thin and soft Biot layers," 67th Annual International Meeting, SEG, Expanded Abstracts , pp.1001-1004.

Biot, M.A., 1956a, Theory of elastic waves in a fluid-saturated porous solid. I. Low frequency range, *J. Acoust. Soc. Am.*, **28**, pp.168-178.

Biot, M.A., 1956b, Theory of propagation of elastic waves in a fluid-saturated porous solid. II Higher frequency range, *J. Acoust. Soc. Am*., **28**, pp.179-191.

Dvorkin, J., Nolen-Hoeksema, R., and Nur, A., 1994, The squirt-flow mechanism: macroscopic description, *Geophysics*, **59**, pp.428-438.

Johnson, D.L., 2001, Theory of frequency dependent acoustics in patchy-saturated porous media, *J. Acoust. Soc. Am.*, **110**(2), pp.682-694.

Johnson, D.L., Koplik, J., and Dashen, R., 1978, Theory of dynamic permeability and tortuosity in fluid-saturated porous media, *J. Fluid Mech*., **176**, pp.379-402.

Myer, L.R., 2001, Fractures as a collections of cracks, *Int. J. Rock Mech. & Min. Sci*., **37**, pp.231-243.

Nakagawa, S., K. T. Nihei, and L. R. Myer, 2004, Plane wave solution for elastic wave scattering by a heterogeneous fracture, *J. Acoust. Soc. Am*., **115**(6), pp.2761-2773.

Nakagawa, S. and M.A. Schoenberg, 2007, Poroelastic modeling of seismic boundary conditions across a fracture, *J. Acoust. Soc. Am*, **122**(2), pp.831-847.

Norris, A.N., 1993, Low-frequency dispersion and attenuation in partially saturated rocks, *J. Acoust. Soc. Am*., **94**, pp.359-370.

Pride, S.R., 2003, Relationships between seismic and hydrological properties, In *Hydrogeophysics*, edited by Y. Rubin and S. Hubbard (Kluwer Acad., New York), pp.1-31.

Pride, S.R. and J.G. Berrymann, 2003a, Linear dynamics of double-porosity and dual-permeability materials, I. Governing equations and acoustic attenuation, *Phys. Rev.E*, **68**, DOI: 10.1103/PhysRevE.68.036603

Pride, S.R. and J.G. Berrymann, 2003b, Linear dynamics of double-porosity and dual-permeability materials, II. Fluid transport equation, *Phys. Rev.E*, **68**, DOI: 10.1103/PhysRevE.68.036604

Schoenberg, M.A., 1980, Elastic wave behavior across linear slip interfaces, *J. Acoust. Soc. Am.*, **68**, pp.1516-1521.

Dutta, N.C., and H. Odé (1979a). "Attenuation and dispersion of compressional waves in fluid-filled porous rocks with partial gas saturation (White Model) – Part I: Biot theory," *Geophysics*, **44**, pp.1777-1788.

Dutta, N.C., and H. Odé (1979b). "Attenuation and dispersion of compressional waves in fluid-filled porous rocks with partial gas saturation (White Model) – Part II: Results," Geophysics, **44**, 1806-1812.

Pyrak-Nolte, L., N.G.W. Cook, and L.R. Myer, 1990, Transmission of seismic waves across single natural fractures, *J. Geophys. Res*., **95**, pp.8516-8538.

Rockhlin, S.I. and Y.J. Wang, 1991, Analysis of boundary conditions for elastic wave interaction with an interface between two solids, *J. Acoust. Soc. Am*., **89**(2), pp.503-515.

Schoenberg, M.A., 1980, Elastic wave behavior across linear slip interfaces, *J. Acoust. Soc. Am.*, **68**, pp.1516-1521.

Table 1. Symbols used in this paper.

| Symbols | Variables |
|---|---|
| $i,j$=1,2,3 | |
| $\omega$ | Circular wave frequency (2π×Hz) |
| $k_i$ | wavenumber |
| $\tau_{ij}$ | Total stress tensor (Pa) |
| $p_f$ | Fluid pressure (Pa) (positive compression ) |
| $u_i$ | Solid frame displacement (m) |
| $w_i$ | Relative fluid displacement (m) |
| $k_{ij}(\omega)$ | 2D fracture permeability tensor ($m^2$) |
| $k_T$ | Isotropic fracture permeability ($m^2$) |
| $\varsigma_T$ | Isotropic fracture permissivity ($m^3$/Pa s) |
| $\phi$ | porosity |
| $K_s$ | Solid (mineral) bulk modulus |
| $K_f$ | Fluid bulk modulus |
| $M$ | (Biot's) Storage modulus (Pa) |
| $\rho_f$ | Fluid density (kg/$m^3$) |
| $\eta_f$ | Fluid viscosity (Pa·s) |
| $h$ | Fracture thickness (for a layer) (m) |
| $h_M$ | Mechanical fracture thickness (m) |
| $h_H$ | Hydraulic fracture thickness (m) |
| $\phi$ | Fracture porosity |
| $\eta_T$ | Shear fracture compliance (m/Pa) |
| $\eta_{Nd}$ | Dry, normal fracture compliance (m/Pa) |
| $\eta_M$ | Material fracture compliance (m/Pa) |
| $\alpha$ | Biot-Willis coefficient |
| $\tilde{B}$ | Fracture Skempton coefficient |

NOTE: The fracture Skempton coefficient is defined via $\tilde{B} = \alpha\eta_{Nu}/\eta_M$ where $\eta_{Nu}$ is the normal compliance of an undrained fracture (Nakagawa and Schoenberg, 2007)

Table 2. Background properties

| Variables | Value |
|---|---|
| Porosity | 0.15 |
| Permeability | $10^{-17}$ $m^2$× or $10^{-11}$ $m^2$ (10μD or 10 D) |
| Solid bulk modulus | 36.0 GPa |
| Fluid bulk modulus | 2.46 GPa |
| Frame bulk modulus | 9.00 GPa |
| Frame shear modulus | 7.00 GPa |
| Solid density | 2,700 kg/$m^3$ |
| Fluid density | 992 kg/ $m^3$ |
| Fluid viscosity | $5.03\times10^{-4}$ Pa·s |
| Tortuosity | 3 |
| Saturation ratio | 1.00 |

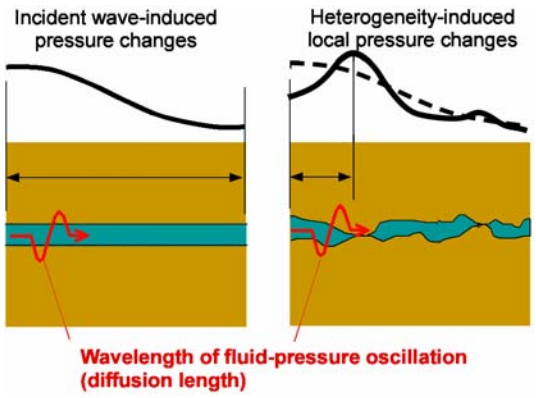


Figure 1. Heterogeneity-induced pressure can result in a steeper pressure gradient within a fracture, which occurs at a scale comparable to or shorter than the pressure diffusion length.

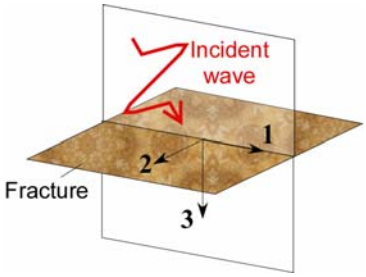


Figure 2. Coordinate system used in the seismic boundary conditions. Incident plane waves are assumed to propagate within the 1,3 plane. We also assume that the fracture is located at $x_3$=0.

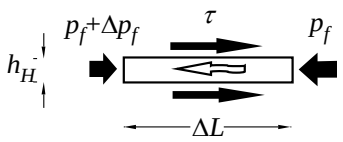


Figure 3. Force equilibrium along a section of a fluid-filled fracture. The effect of inertia is neglected.

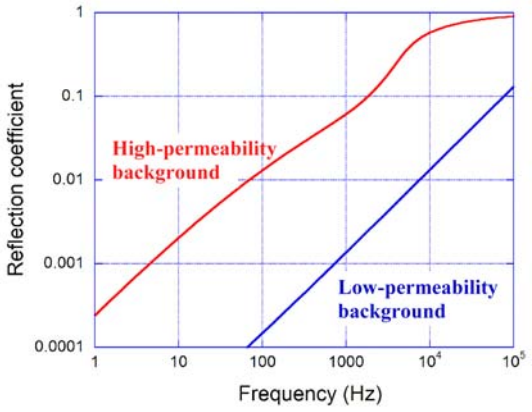


(a) Normal incidence

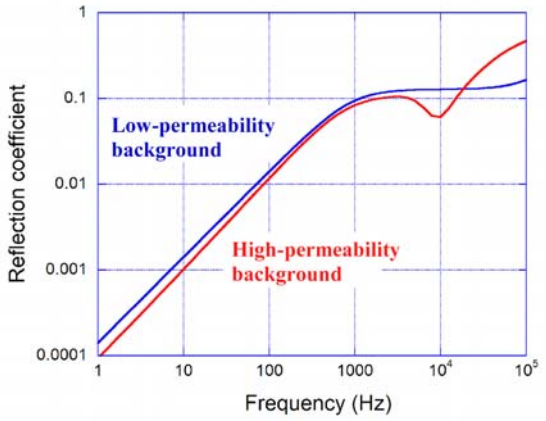


(b) Oblique incidence (45$^o$)

Figure 4. Reflection coefficients of fast P waves for a water-saturated, homogeneous fracture

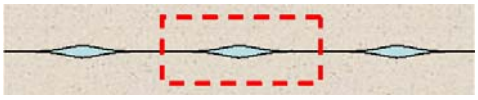

Figure 5. One-dimensional, periodic, heterogeneous fracture model

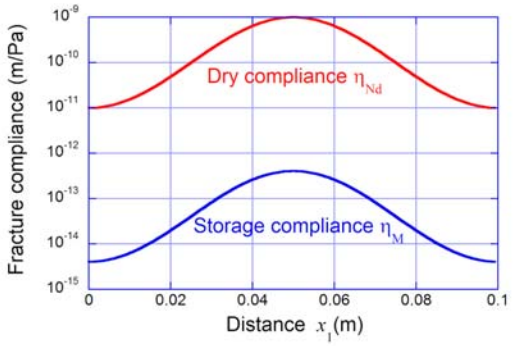


Figure 6. Fracture compliance distribution for a water-saturated, heterogeneous fracture. (Note: shear compliance is identical to the dry, normal compliance.)

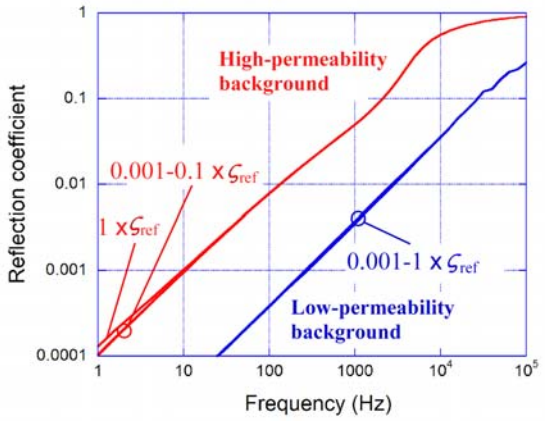

Figure 7. Normal-incidence reflection coefficients of fast P waves for a water-saturated, heterogeneous fracture

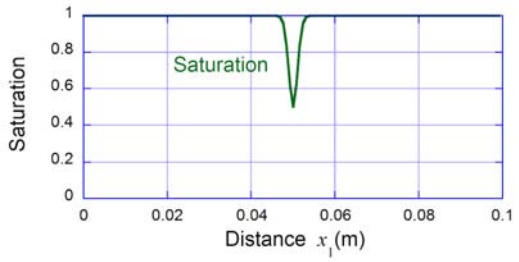


Figure 8. Saturation profile of a partially saturated, water-filled fracture

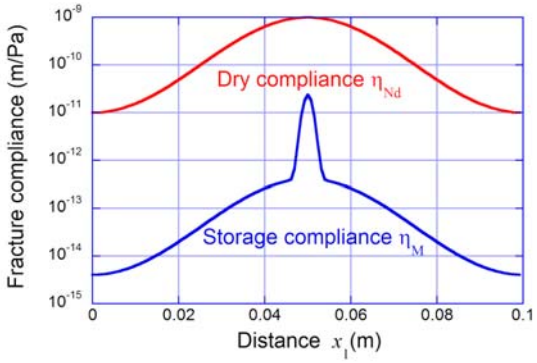


Figure 9. Fracture compliance distribution for a partially saturated, water-filled fracture

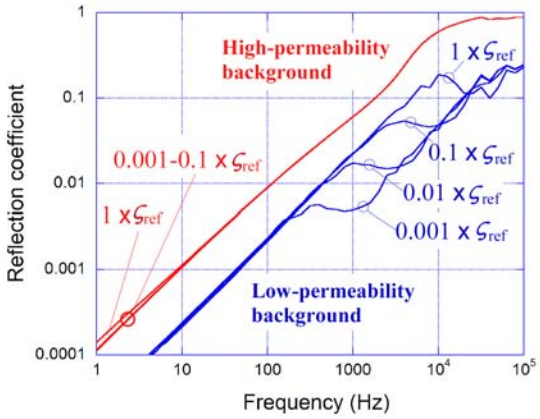


Figure 12. Reflection coefficients of fast P waves for partially water-saturated, heterogeneous fracture

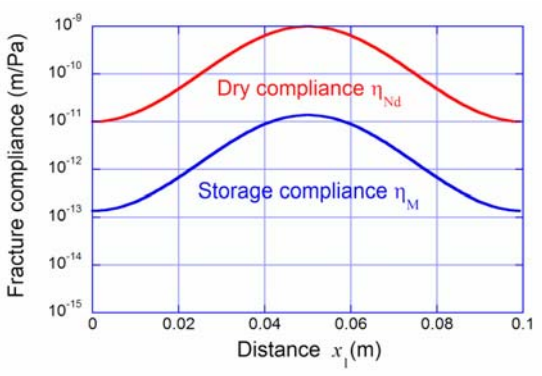


Figure 11. Fracture compliance distribution for a supercritical $CO_2$-saturated heterogeneous fracture

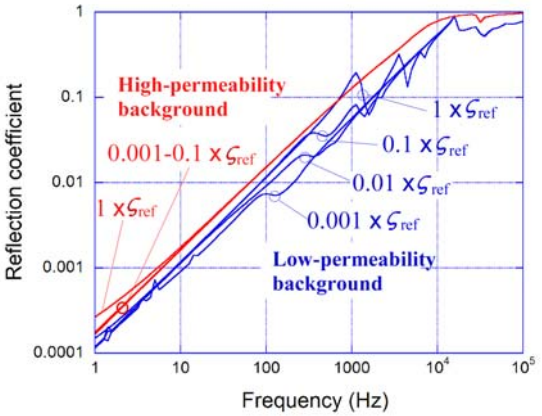


Figure 12. Reflection coefficients of fast P waves for a supercritical $CO_2$-saturated, heterogeneous fracture

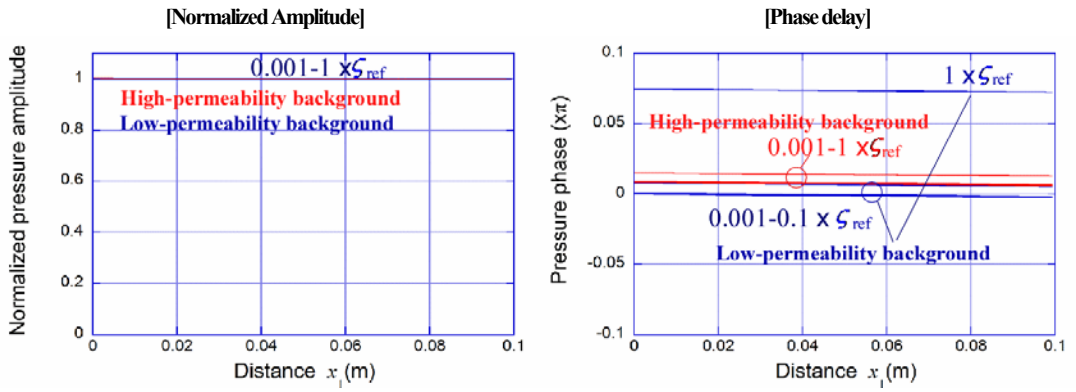


(a) Homogeneous, water-saturated fracture; 45° incidence

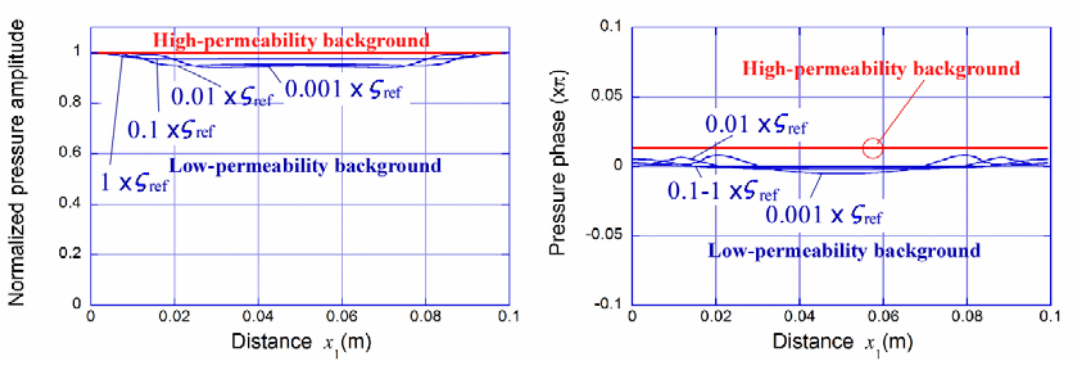


(b) Heterogeneous, water-saturated fracture; Normal incidence

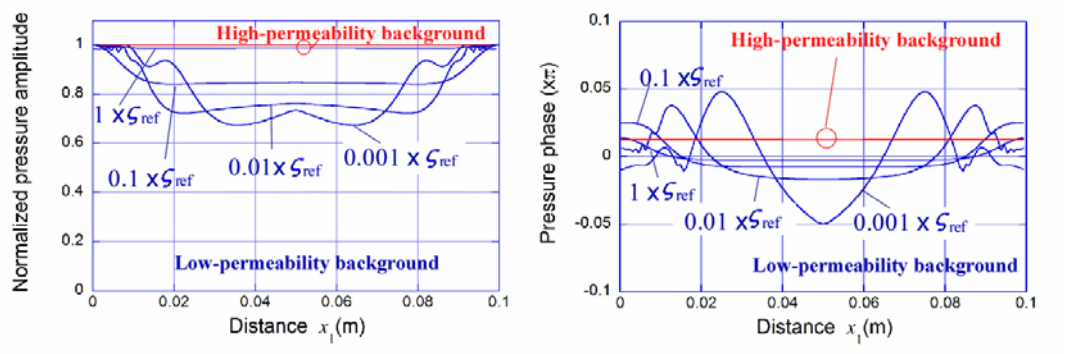


(c) Heterogeneous, partially water-saturated fracture; Normal incidence

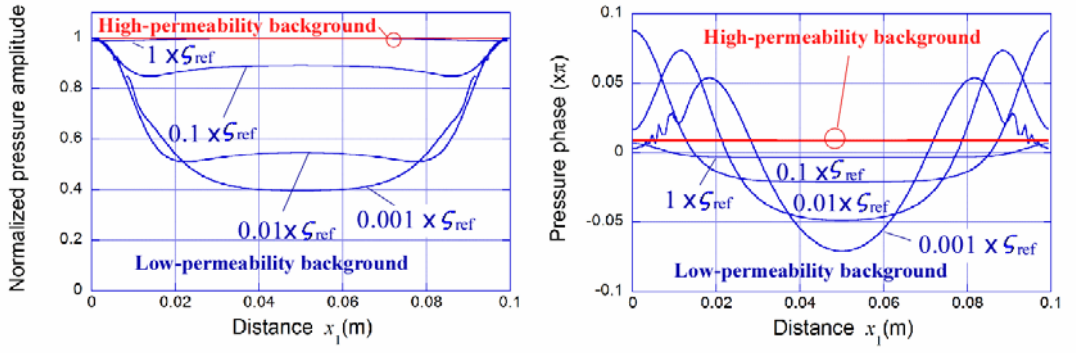


(d) Heterogeneous, $CO_2$-saturated fracture; Normal incidence

Figure 13. Fluid pressure distribution within a fracture at 316 Hz. The amplitudes are normalized to the maximum amplitude for each profile.

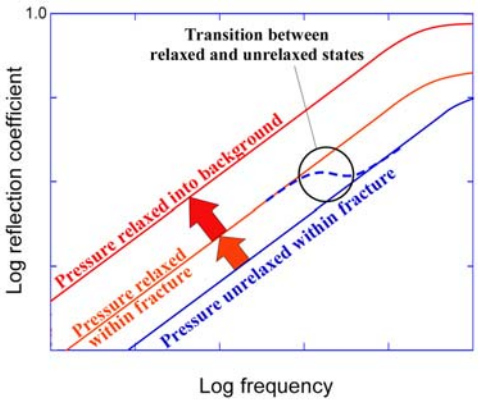


Figure 14. Effect of background and fracture permeability on the reflection of fast P waves